Astronomy & Astrophysics manuscript no. 9347
16th April 2008

The nearest X-ray emitting protostellar jet (HH 154) observed with *Hubble*⋆

R. Bonito[1,2,3], C. V. M. Fridlund[4], F. Favata[5], G. Micela[2], G. Peres[1], A.A. Djupvik[6], and R. Liseau[7]

[1] Dip. Scienze Fisiche ed Astronomiche, Sez. Astronomia, Università di Palermo, P.zza del Parlamento 1, 90134 Palermo, Italy
[2] INAF – Osservatorio Astronomico di Palermo, P.zza del Parlamento 1, 90134 Palermo, Italy
[3] COMETA, via S. Sofia, 64 95123 Catania, Italy
[4] Astrophysics Div. – Research and Science Support Dept. of ESA, ESTEC, Postbus 299, 2200 AG Noordwijk, The Netherlands
[5] European Space Agency Community Coordination and Planning Office 8-10 rue Mario Nikis F-75738 Paris cedex 15 France
[6] Nordic Optical Telescope Apartado 474 E-38700 Santa Cruz de La Palma Santa Cruz de Tenerife, Spain
[7] Onsala Space Observatory SE-439 92 Onsala, Sweden

Received, accepted

Abstract

Context. The jet coming from the YSO binary L1551 IRS5 is the closest astrophysical jet known. It is therefore a unique laboratory for studies of outflow mechanisms and of the shocks occurring when expanding material hits the ambient medium as well as of how the related processes influence the star- (and planet-) forming process.
Aims. The optical data are related to other data covering the spectrum from the optical band to X-rays with goal of understanding the energetics of low-mass star jets, in general, and of this jet in particular. We study the time evolution of the jet, by measuring the proper motions of knots as they progress outwards from the originating source.
Methods. The nebulosities associated with the jet(s) from the protostellar binary L1551 IRS5 were imaged in a number of spectral bands using the Hubble Space Telescope. This allows the proper motion to be measured and permits a simple characterization of the physical conditions in different structures. To this end we developed a reproducible method of data analysis, which allows us to define the position and shape of each substructure observed within the protostellar jet. Using this approach, we derive the proper motion of the knots in the jet, as well as their flux variability and shock emission.
Results. The time base over which HST observations were carried out is now about ten years. The sub-structures within the jet undergo significant morphological variations: some knots seem to disappear in a few years and collision between different knots, ejected at different epochs and maybe with different speed, may occur. The velocities along the jet vary between $\sim$ 100 km s^{-1} and over 400 km s^{-1}, with the highest speed corresponding to the knots at the base of the jet.
Conclusions. There are indications that the HH 154 jet has been active relatively recently. Our results suggest the presence of a new shock front at the base of the jet identified with an internal working surface. From the analysis of the terminal and internal working surfaces within the jet, we find that the more likely scenario for the HH 154 jet is that of a jet traveling through a denser ambient medium (a "light jet"). These results are consistent with the Bonito et al. (2007) model predictions. Furthermore, there is strong evidence that the knots at the base of the northern jet correspond to the location where the highest velocity and the highest excitation component are measured along the jet. More important, this is the location where the X-ray source has been discovered.

Key words. Shock waves; ISM: Herbig-Haro objects; ISM: jets and outflows; X-rays: ISM

1. Introduction

The L1551 star-forming region is located in the Taurus molecular complex, making it one of the closest (about 150 pc) to us (Kenyon et al. 1994). It demonstrates all signs of low-mass star formation taking place in the recent past or ongoing. Several molecular outflows and jets, the most remarkable being the one centered on the binary young stellar object IRS5, are found along with a number of T-Tauri stars, X-ray sources, Herbig-Haro objects, protostellar disks, and embedded sources. The outflow centered on IRS5 is one of the most studied and was the first to be identified (Snell et al. 1980). IRS5 is a binary system (Bieging & Cohen 1985; Rodriguez et al. 1986; Looney et al. 1997, Rodríguez et al. 1998) with star masses of approximately $0.8\ M_{\odot}$ and 0.3 (Liseau et al. 2005). Each of the components is

Send offprint requests to: R. Bonito
e-mail: sbonito@astropa.unipa.it

⋆ Based on observations made with the NASA/ESA Hubble Space Telescope, obtained at the Space Telescope Science Institute, which is operated by the Association of Universities for Research in Astronomy, Inc., under NASA contract NAS 5-26555. These observations are associated with programs #6127, #6411 & #10351

surrounded by a small (∼10 AU) disk (Rodríguez et al. 1998), and the complex is enveloped in a larger (∼5000 AU), dense, flattened, and rotating structure (Fridlund et al. 2002). An optical jet with Herbig-Haro characteristics (designated HH 154 jointly) originates in each of the stellar components (Fridlund & Liseau 1998; Rodríguez et al. 2003) behind the ≈ 150 magnitudes of visual extinction that surrounds the binary, the first knot being at about $0\farcs5$ from the star.

HH 154 is among the known astrophysical jets located nearest to the Earth. Earlier ground-based data has made it clear there is a need for higher spatial resolution than achieved from the ground, to resolve the shock structure of the knotty pattern of the jet. The NASA/ESA Hubble Space telescope (HST) can achieve similar spatial resolution to the current 2D hydrodynamical calculations of jets ($\sim 10^{14}$ cm). A multi-cycle observing program with the HST consequently has appeared strongly motivated to study of time evolution of the jet using the shock diagnostic emission lines of H_α and the [SII] doublet at $\lambda\lambda 6717, 6731$Å to determine its physical properties.

As we discuss in the following, it is feasible to detect the proper motion of the knots within the jet. The relatively rapid evolution of knots within the jet (time scale of a few years), as well as the expansion of the jet (almost doubling in length during the 3 decades that it has been observed), is indicative of space velocities on the order of 500 km s^{-1}(Fridlund et al. 2005, FL05 hereafter). In principle, shocks occurring at these velocities could generate an observable X-ray flux. Favata et al. (2002) discovered X-rays emanating from the jet in the area that includes both the jet and the shock-induced nebulosities, within the blue-shifted lobe, by using the ESA XMM-Newton X-ray telescope. This and a later observation (Favata et al. 2006), along with the data of Bally et al. (2003), have demonstrated that the X-rays do origininate in the jet itself and not from the coronal activity of the IRS5 system. The source is placed where the dual jet emerges from behind the compact obscuration, i. e. about $0\farcs5$ – $1\farcs0$ away from IRS5 itself. Furthermore the X-ray spectrum and proper motion together provide a self-consistent scenario: the first gives a best-fit temperature of 4 MK, consistent with a shock speed of 500 km/s, and the second (proper motion) gives about 500 km/s. The location of the X-ray source coincides with the position where optical spectroscopy and HST imaging finds nebular knots that have space velocities in excess of 500 km/s (FL05).

Detailed hydrodynamic numerical modeling by Bonito et al. (2004, 2007) has shown that the X-ray emitting shocks should be moving at speeds of $\approx$ 500 km/s, consistent with the observed velocities. In this context, Bonito et al. (2007) found that the high spatial resolution of the *Chandra* observatory would allow detection of the *X-ray source proper motion* with a time base of only a few years. Favata et al. (2006) thus carried out such observations, in conjunction with another set of HST imaging, increasing the time base of the HST observations of the HH 154 jet from two years to nine years, and the total time base of high-quality data, ground-based and space-borne, also considering the older data from the literature (e.g. Neckel & Staude 1987), now covers over thirty years. The new X-ray data have been reported elsewhere but, in summary, Favata et al. (2006) find that the X-ray source has indeed undergone a temporal evolution. Reducing the original *Chandra* data (obtained in 2001) of Bally et al. (2003), consistently with data from 2005, one finds in 2001 mainly an unresolved point source, with a possible slight extension in the downstream direction. In the 2005 data, this has evolved such that the unresolved component has remained stationary, while the extended component has continued to move downstream as expected from a shock moving away from the IRS5 binary. The implied velocity of the X-ray moving shock is 460 km/s, in excellent agreement with the modeling of Bonito et al. (2004, 2007).

In the present paper we report the analysis of HST data from 1996, 1998, and 2005 observations. We again reduced the complete set of HST data for a self consistent treatment of all the data. Our aims include the study of the proper motion of the protostellar jet as a whole and of each small structure within the jet (optical knots) by comparing the HST observations of HH 154 taken at various epochs and to infer whether it is possible to relate the dynamics and energetics of the optical structures within the jet with the complex morphology of the X-ray source discovered at the base of the jet (Favata et al. 2006). Also, following Hartigan (1989), the multi-wavelength (H_α and [SII]) analysis of the shocks within the protostellar jet allows us to constrain the relevant physical properties of the jet/ambient system, so as to test the numerical model predictions of Bonito et al. (2004, 2007).

In Sect. 2 we report the data and method developed for the analysis. In Sect. 3 we present the results for the morphological variation of the structures within the jet, their emission in both H_α and [SII] filters, the proper motion of each knot, and their flux. And finally our conclusions are drawn in Sect. 4.

2. Observations and data reductions

The region centered on L1551 IRS5 jet has been imaged using the Wide Field and Planetary Camera 2 (WFPC2) onboard the *Hubble Space Telescope* in 1996, 1998, and 2005. This camera consists of four adjacent 800×800 pixels CCDs. Of these, the WF2-4 have a plate scale corresponding to 0.0996"/pix, while the PC1 chip has better resolution, corresponding to 0.0455"/pix. As in the case of the previous 1996 and 1998 observations (FL05), we centered the jet (whose total length[1] is currently $\approx 10''$) in the PC camera, using an orientation of the WFPC2 camera allowing the registration of the only observable star (VSS 4, Vrba et al. 1976) within the WFPC2 field-of-view, on the WF4 chip.

The 1996 (1996.034), 1998 (1998.074), and 2005 (2005.021 and 2005.022) observations consist of two exposures for each filter *F656N* (H_α) and *F673N* ([SII] doublet: $6717, 6731$Å). Dividing each exposure into sub-exposures to be able to clean the images from cosmic ray hits, we achieved a total exposure time of 2005 s, 2600 s, and 2400 s for each filter in 1996, 1998, and 2005, respectively (see Table 1).

[1] In this paper we refer to dimensions projected on the plane of the sky. Note that the inclination of the HH 154 jet is almost equal to 45° (FL05).

Table 1. Information about the 1996, 1998, and 2005 data in both filters.

obs. ID	date	exposure time (s)	filter
u31f0107t	1996 Feb 03	1300	[SII]
u31f0108t	1996 Feb 03	1200	[SII]
u31f0109t	1996 Feb 03	1300	H_α
u31f010at	1996 Feb 03	1200	H_α
u3nj0101r	1998 Mar 15	1300	[SII]
u3nj0102r	1998 Mar 15	1300	[SII]
u3nj0103r	1998 Mar 15	1300	H_α
u3nj0104r	1998 Mar 15	1300	H_α
u9570201m	2005 Jan 22	1200	[SII]
u9570202m	2005 Jan 22	1200	[SII]
u9570101m	2005 Jan 21	1200	H_α
u9570102m	2005 Jan 21	1200	H_α

Data reduction follows the standard methods discussed in detail in Heathcote et al. (1996) and in the WFPC2 handbook. Briefly, we used the IRAF/STSDAS software environment to remove the warm pixels in WFPC2 CCDs (using the STSDAS task **warmpix**). This is an important step because one of our aims is to estimate the fluxes of faint extended sources that could be modified by the presence of such hot pixels. An analogous problem could arise in the case of cosmic ray events near the sources we want to analyze. To avoid errors in computing fluxes due to the influence of cosmic ray emission, we remove the cosmic rays by using the STSDAS task **crrej** in the two exposures for each filter for the three epochs. Because cosmic ray events are very numerous in long exposures, several pixels are affected by double hits, which cannot be removed by running the crrej task (which just compares the two exposures), so we need to identify cosmic rays and to remove them in each image.

The images were interpolated across bad pixels using the STSDAS task **wfixup** and mosaics obtained of all four detectors images of WFPC2 using the STSDAS task **wmosaic**, which takes chip distortions and rotation into account and reduces the PC field to the same resolution as the three WF images. The resulting mosaics are for illustration purposes only. All the quantitative results and measurements were derived by the single chip images (in particular those concerning the structures detected in the high resolution camera, PC).

The short-term focus variations due to temperature changes as the telescope warms up during its orbital day and cools down during orbital night, usually referred to as "HST breathing", cause effects at the 0.01 pixel level (Anderson & King 2003). Since we assumed that the accuracy in the determination of the shift between different epochs images is close to 0.1", which corresponds to about 1 pixel, the breathing effect is negligible and does not affect the precision of proper motion determination in this work.

What is new in our analysis, especially compared to the procedure of FL05, is the method used to register the images and to define the apertures around each structure within the jet. First of all, we align the images in the three epochs by using the World Coordinate System in SAOImage ds9. In this way we rotate the image so as to have north up and east on the left of the image (analogous to rotating the figure by the value of the header keyword ORIENTAT), and for each camera we register the position of the center coordinate of the pointing. As a next step, we find the position of the VSS4 star in the WF4 chip for both filters in the three epochs. From a comparison of the positions of the star in 1996, 1998, and 2005, we have found an offset, which we account for in registering the multi-epochs observations. Furthermore, the VSS4 star shows a significant proper motion (Cudworth & Herbig 1979) that, in nine years, i.e. the time baseline between 1996 and 2005 observations, amounts to (+0$''$.13,-0$''$.49). We have taken the proper motion of VSS4 into account, together with the offset found between the multi-epoch observations in the position of VSS4 in the WF4 chip to register the images, in order to compute the proper motion of each substructure within the jet. The accuracy in the shifts measured between 1998 and 2005 images with respect to the 1996 position of the VSS 4 star in WF4 chip is ~ 0.1" due to the resolution of the camera.

To identify each structure within the jet in both filters and in each epoch, we tested several criteria for the choice of the contours defining each knot. The position of these contours will allow us to define the position of each knot and, as a consequence, to derive the proper motion of the knots by comparing the multi-epochs images in both filters, as discussed in Sect. 3.3. First, we used contours at a fixed fraction of the maximum flux in each knot. Noting that the value of the maxima are different for different structures (i. e. the maximum is a local property of each knot), we decided not to use such a procedure as a definition of the contours around the structures. On the other hand, the value of the background also varies, up to a factor four between the 1996, 1998, and 2005 images, so we have chosen not to use contours at multiples of σ, $k\sigma$, with respect to the background to identify the structures. These considerations led us to choose a fixed threshold for the contours in each epoch. In particular we find that, in 1996, 1998, and 2005 H_α images of HH 154, the knots within the jet are well-defined as separated structures if contours enclosing a region with 3 cnts/pix are used. This makes sense because the exposure time is almost the same across the whole set. Furthermore, we define the σ as: $\sigma = \sqrt{F_{sky}}/A_{tot}$, where F_{sky} is the sum of all the counts within 8 identical circular areas, of 2" radius, sampling 8 different regions without any source, and A_{tot} is the sum of the 8 areas on the sky. With this definition, our σ refers to the total number of counts within the area encircled by the contours, and 3 cnts/pix corresponds to contours at about 1000σ, 500σ, and 600σ with respect to the background for the 1996, 1998, and 2005 H_α data, respectively.

The approach that we have chosen for identifying the substructures within the jet and described above allows a quantitative and reproducible definition of the contours on each knot in protostellar jets.

The contours used to define the knots within the jet are also used to measure the total flux of each structure. In particular, we compute the total flux within the contour on each knot. This value also takes a contribution due to the sky into account. To derive the flux associated to the knot itself, we subtract the background by estimating the value of the sky within the same contour, simply moving the same aperture defining the knot

in a region where no other sources (knots or cosmic rays) are located. This procedure implies that any bias level removal is unnecessary. The comparison of the multi-epochs estimates of fluxes will allow us to derive information about the energetics of the substructures within the jet and of the jet as a whole as well. Photometric calibration is made following Holtzman et al. (1995) calibration for narrow-band filters.

Figure 1 shows the HH 154 jet observed with HST in 1996 in the H_α filter. The contours that identify the knots within the jet, as well as the nominal position of the protostar IRS5, are superimposed on this figure.

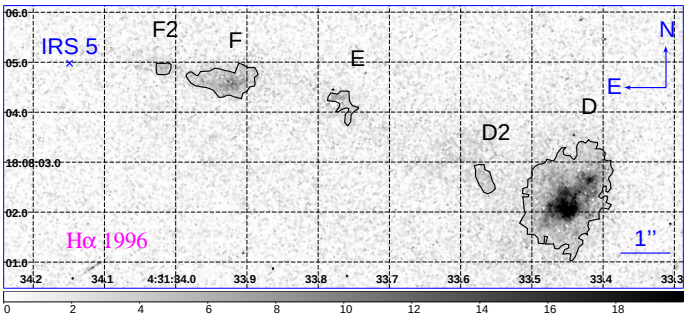

Figure 1. The HH 154 jet observed with HST in 1996 in the H_α filter. The contours defining the knots within the jet and the nominal position of the IRS5 system are superimposed on the figure.

3. Results

3.1. Morphological changes

In Fig. 2, we show the 1996 HST observations of the HH 154 jet in the H_α (left panel) and [SII] (right panel) filters. The contours defining each knot within the jet are also shown superimposed on this figure (1996 in blue, 1998 in green, and 2005 in red). The jet consists of two separate components ('northern jet' and 'southern jet') as is clear from the I- and R-band representations in FL05. As suggested by Fridlund & Liseau (1998), each of these two jets can come from one of the two components of IRS5 found by Looney et al. (1997) and by Rodríguez et al. (1998). This structure is, however, not immediately evident in Fig. 2, but it is evident from the R image of the 1996 HST observations of the HH 154 jet (Fig. 3). The emission from the southern jet is fainter than the more active northern jet; even the knots observed at the end of the fainter jet have emission several orders of magnitude lower than those at the head of the northern jet.

The knotty structure within the jet is evident in Fig. 4, which shows a cut of the count image along the axis of the northern jet in the H_α filter in 1996. The dominant substructures within the jet are located at the base and at the head of the jet, 'F-complex' and D knot (nomenclature of FL05), respectively.

The HH 154 jet emerges from the highly obscured (≈ 150 mag) region surrounding the driving source IRS5, and the first visible structure at the base of the jet is the 'F-complex' (see enlargements of the base of the jet in H_α and [SII] in Fig. 5).

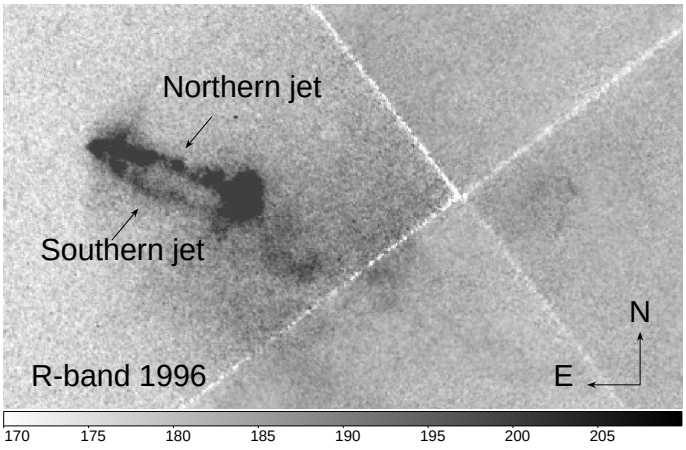

Figure 3. R-band image of the HH 154 southern and northern jets in 1996.

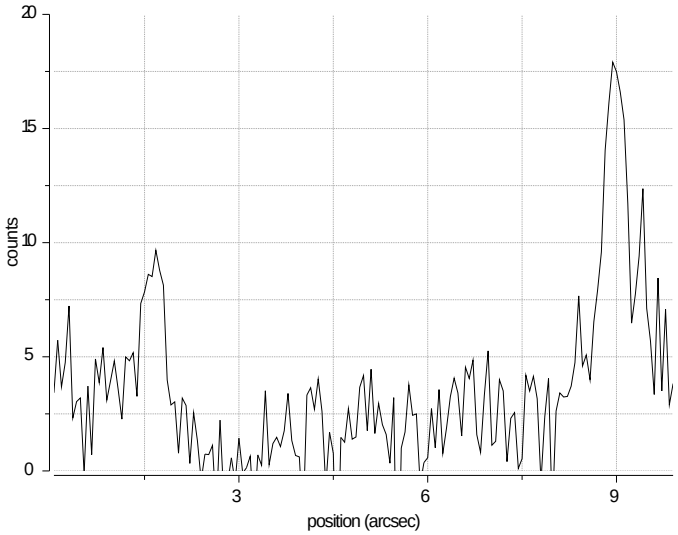

Figure 4. Cut along the northern jet axis of the count image in the H_α filter in 1996. The origin is located at the base of the jet, where the F_2 knot originates.

It consists of two knots, F_2 and F, merging in a single stretched structure as it evolves.

From Fig. 5 the variation in the morphology of the F-complex over the years and with wavelength is evident. First of all, knot F_2 seems to approach knot F with time. Furthermore, the whole F-complex evolves as a single elongated structure in the new 2005 observations. At this position, the extinction is between 4.5 and 6 magnitudes in V, while it is significantly more at the very base of the jet.

The middle section of the jet (E and D_2 knots) is very faint in the 2005 HST data and devoid of large structures, and a trend is clearly seen in the images over the period covered by HST observations, especially in the 2005 observations. In a similar way as in the case of the F-complex discussed above, the knots in the middle part of HH 154 show changes in emission and have variable morphology. The faint structures within the middle portion of the HH 154 jet, knot E (near the F-complex) and knot D_2 (near the terminal working surface, knot D), seem to

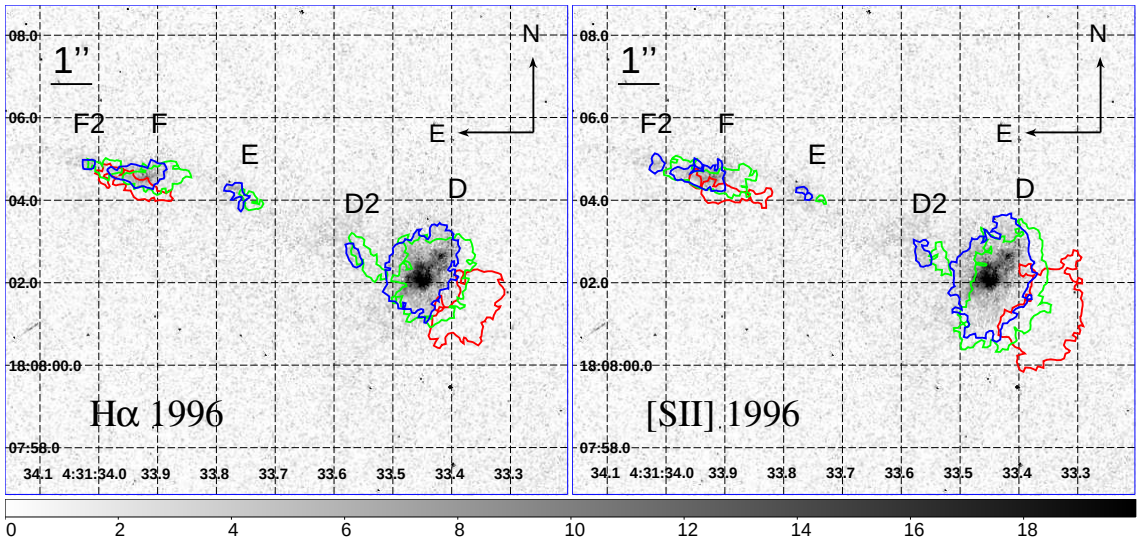

Figure 2. HST image of the HH 154 jet in 1996 in both the H_α (left panel) and [SII] (right panel) filters. The superimposed contours define the knots within the jet at different epochs: 1996 (blue), 1998 (green), and 2005 (red).

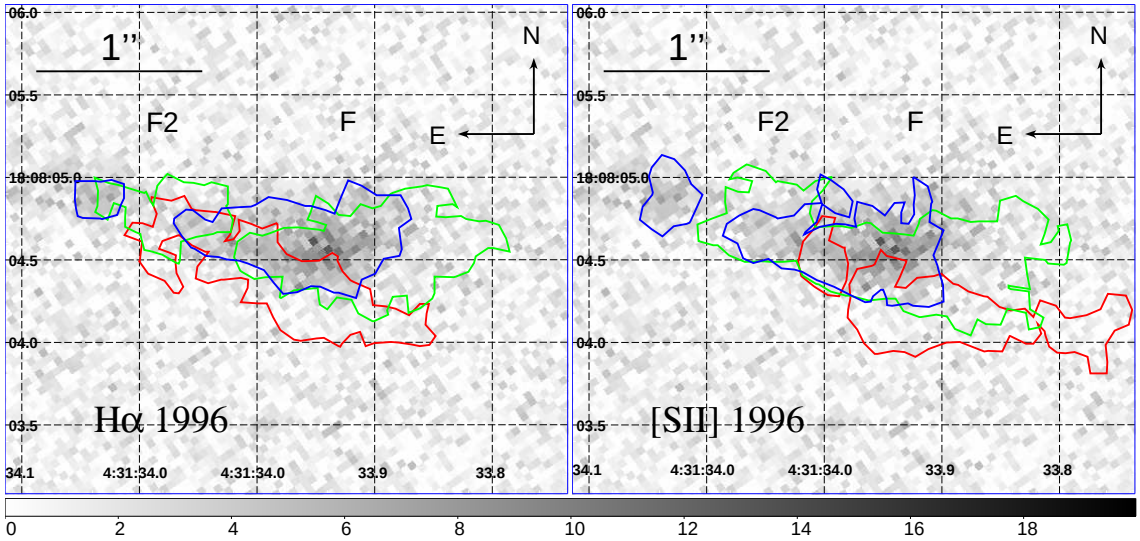

Figure 5. Enlargement of the F-complex at the base of the HH 154 jet in 1996 in H_α (left panel) and [SII] (right panel). Contours for the identification of knot F_2 (on the left) and F (on the right) in different epochs (1996 in blue, 1998 in green, and 2005 in red) are superimposed on this figure.

become fainter and fainter, vanishing in the 2005 observations, or maybe decomposing into several sub-knots, remnants of previous individual knots (see Fig. 6) or merging with other structures. Comparing with the results of Neckel & Staude (1987) covering the years 1983-1987, the E knot is the second brightest feature, and it is obvious that it is moving closer to knot D. It is possible that the vanishing feature D_2 (see below) is a remnant of this feature, while the knot E is a more or less stationary weakening shock at the location of the original (1983) feature.

The brightest knot within the HH 154 jet, knot D, is located at the head of the jet (far from the source IRS5, from which the jet originates) and can be identified with the terminal working surface, where the jet interacts with the surrounding medium. The morphological changes of the spatial structures are quite visible not just within the jet as a whole, but even within each small structure (optical knots). This is evident in the case of knot D, as shown in Fig. 7, where a shift of the brightest spot within the knot itself is detectable. We measured this shift within the knot D deriving a value of about $1''$ in the NW direction in about nine years (it was about $0.3''$ between 1996 and 1998), in the knot's reference system (see Fig. 8), while the D knot, with the total jet, is moving in the SW direction as a whole. Details on the value of the maximum of the brightest spot within the D knot and on its position in H_α images in 1996, 1998, and 2005 are summarized in Table 2. Feature D_2 appears to be merging with the working surface, knot D. The process continues and the 2005 HST observations show no presence of this knot near the working surface D. This could have influenced the detectable movement of the brightest spot observed within the knot D in the NW direction.

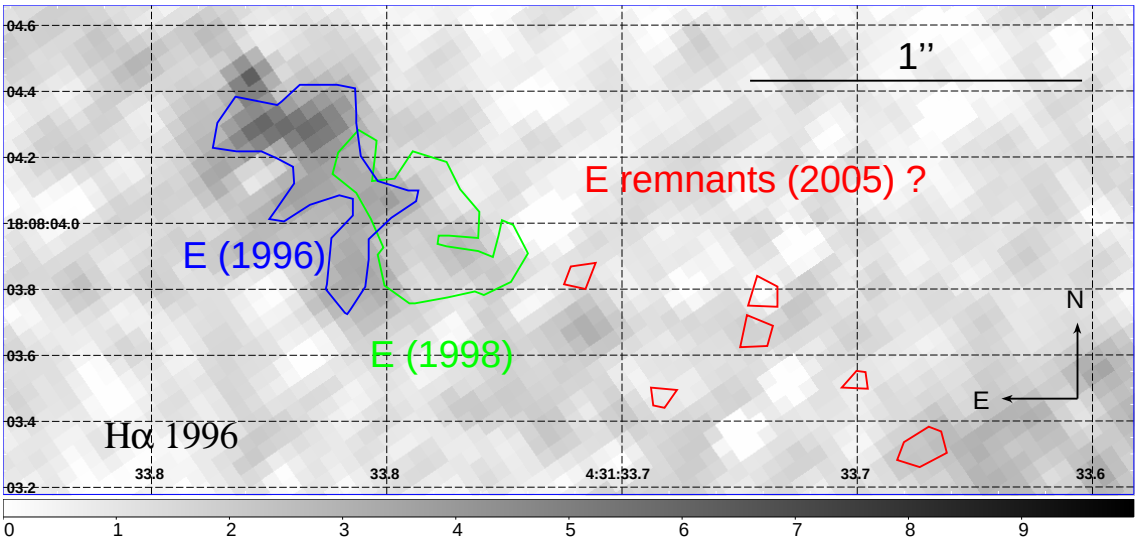

Figure 6. The E knot in the 1996 observation in the H_α filter with the contours that define the knot in 1996 (blue), 1998 (green), and (2005). In 2005 this knot was disappearing or decomposing into several remnants.

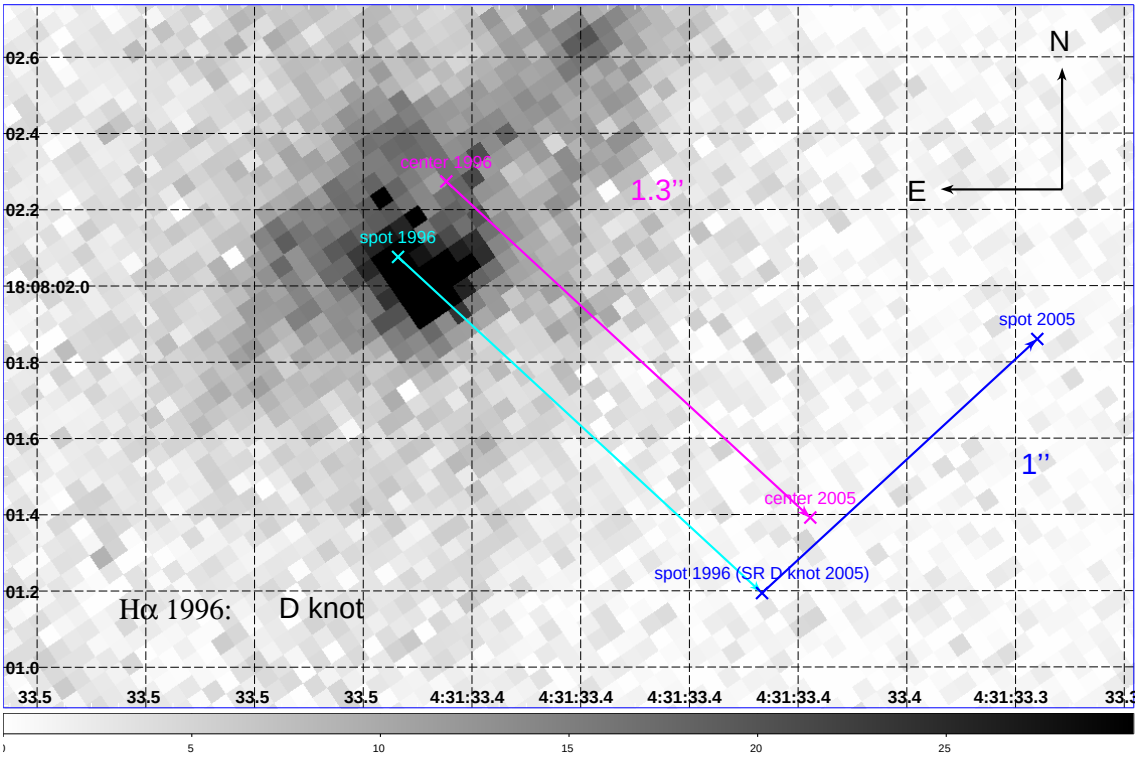

Figure 8. Enlargement of the D knot at the head of the jet: the motion of the brightest spot within the knot (blue vector) is measured in the reference system of the center of the D knot.

3.2. H_α and [SII] structure

The H_α emission identifies the position of the shock; in fact, collisional excitation of neutral atoms entering the shock marks the physical location of the shock front itself. On the other hand, the cooling zones behind the shock front mainly emit forbidden-line radiation, such as [SII]. Hence the stratification of the H_α and [SII] emission makes it possible to recognize the location of two very different physical regions within protostellar jets.

To this end in Fig. 9, we show the difference image H_α - [SII] of the HH 154 jet as a whole as observed with HST in 2005. As pointed out by Fridlund & Liseau (1998), the difference image results in the cancellation of the jet, leading to the conclusion that the central part of the jet is of intermediate excitation ([SII]/H_α < 1.5, Raga et al. 1996). At the spatial resolution of HST/WFPC2, we expect to be able to resolve the shock structure of the brightest knots. The working surface generally consists of two shocks, the bow shock and the Mach disk, marked by the H_α emission, and of a cooling zone (be-

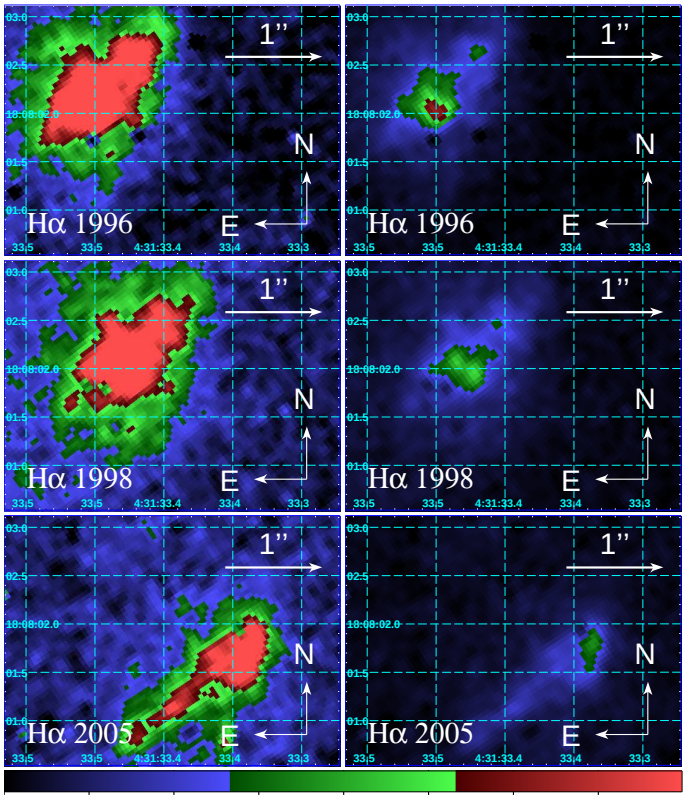

Figure 7. Enlargement of the terminal working surface, knot D, at the head of the HH 154 jet in 1996 (upper panels), 1998 (middle panels), and 2005 (lower panels) in H_α, at two different contrast levels: high contrast (on the left) to show the fainter features and low (on the right) to show the brighter features.

Table 2. Position, proper motion, and value of the maximum corresponding to the bright spot within the D knot evaluated from the H_α images in 1996, 1998, and 2005.

yr	max (cnts)	α (J2000.0)[a]	δ (J2000.0)[b]	v@150 pc (km/s)
1996	37.2284	04 31 33.454	+ 18 08 02.08	-
1998	29.6317	04 31 33.422	+ 18 08 01.97	120[c]
2005	20.6488	04 31 33.336	+ 18 08 01.86	80[d]

[a] Units of α: hours, minutes, and seconds
[b] Units of δ: degrees, arcminutes, and arcseconds
[c] In the reference frame of the D knot in 1998
[d] In the reference frame of the D knot in 2005

tween the shocks) marked by the [SII] emission. The bright and dark structures in the difference image in Fig. 9 are indicative of a stratification in the two different emission, H_α and [SII], corresponding to the two different physical zones, the shock front and the post-shock region in the particular case of the HH 154 jet.

In particular, in Fig. 9 there is no evidence of H_α emission marking the forward shock (bow shock) expected to be farther away from IRS5 than the location of the cooling zone marked by the [SII] emission. This result will be discussed in Sect. 4. H_α emission of the brightest knot, the D knot, appears to vary from an almost ellipsoidal blob in both 1996 and 1998 HST observations (see upper and middle panels in Fig. 7) to the most elongated structure observed in 2005 (see lower panels in Fig. 7). This stretched blob is evident in the difference image H_α - [SII] derived from 2005 observations (Fig. 9). Here the [SII] cooling region appears to wrap around the H_α emitting region corresponding to the reverse shock. The structure of the difference emission H_α - [SII] and its implications are discussed in Sect. 4.

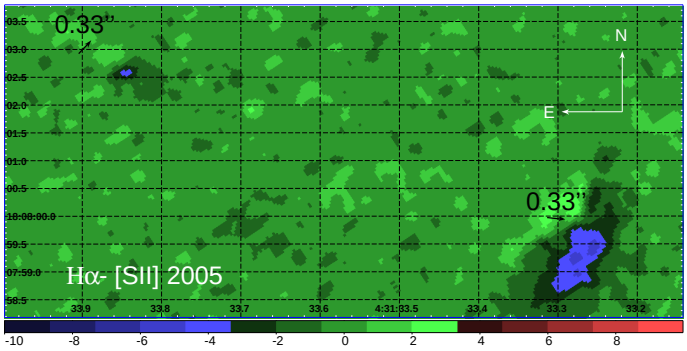

Figure 9. Difference image H_α - [SII] of HH 154 as observed with HST in 2005. The arrows indicate the dimension of the jet radius at its base and the separation between the center of the contour on the D knot in H_α and in [SII], both equal to about $0.33''$.

A similar structure seems to be present at the position corresponding to the F-complex at the base of the jet, where the jet velocities reach their maximum value (FL05). This could be evidence of a new shock formed near the parent stars, and it is the place where X-ray emission has been detected with Chandra (Bally et al. 2003; Favata et al. 2002).

3.3. Proper motion

The three different HST observations of HH 154 in three epochs (1996, 1998, and 2005) allowed us to perform proper motion measurements with a time base of about two years and of about nine years, i. e. to derive average velocities over nine years, comparing the 1996 and 2005 HST data sets, and almost "instantaneous" velocities over two years, from the 1996 and 1998 observations. Figure 10 shows the RGB images in both the H_α and [SII] filters of the HH 154 jet in the three epochs (1996 in blue, 1998 in green, and 2005 in red): the motion of the knots is evident.

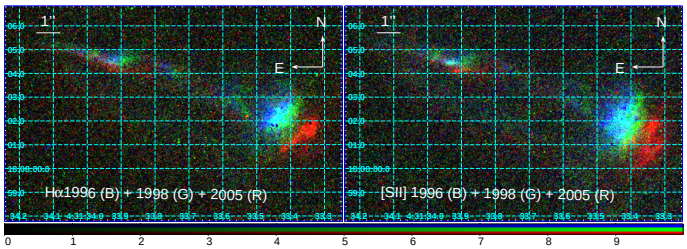

Figure 10. RGB image in the H_α and [SII] filters of the HH 154 jet in the three epochs (1996 in blue, 1998 in green, and 2005 in red).

The only structure identifiable over the complete time span of 25 years, since the original observations of Neckel & Staude (1987) is the working surface, knot D, and dramatic changes take place within that feature itself as we show convincingly below. The contours defining the knots within the jet are chosen following the method described in Sect. 2 and are shown in Fig. 2.

Once a criterion for the identification of each knot has been chosen, as discussed in Sect. 2, we can derive the position of the center of the contours defining the knots. To calculate the center of a polygon, one sums the vector for each vertex and then divides by the number of vertexes[2]. Note that the position of the center of the contour does not necessarily correspond to the position of the maximum of the knot within the contour. As a consequence, the proper motion of the D knot, computed by considering the position of the center of the contour, does not account for the motion of the brightest spot within the D knot itself. Our choice of the contours leads to the definition of a single structure consisting of both knots F and F_2 in the [SII] image in 1998 and H_α image in 2005 (see Fig. 5). In this case we compared the position of the maxima corresponding to each knot separately to compute the proper motion. Table 3 summarizes the displacements of each knot in about two (from 1996 to 1998) and nine years (from 1996 to 2005) in both filters and the corresponding velocity. As explained above, for knots F and F_2 we use the position of the maxima within the contours ("max" in the column "Comment" of Table 3) instead of the position of the center ("center" in the column "Comment" of Table 3) of the contours. Note that we consider different values of the velocity in the H_α and [SII] filters as these two emissions refer to different physical regions, as explained in Sect. 3.2.

We can only compare the average speeds derived over nine years, from 1996 to 2005, with the "instantaneous" speeds derived over two years from 1996 to 1998. It would be very interesting to perform new HST observations of the HH 154 jet in the next few years so as to be able to compare "instantaneous" velocities. This comparison would allow us to infer detailed information on the dynamics of the protostellar jet, the deceleration of its knots being one of the main topics. Figure 11 shows the proper motion of the knots within the jet (identified by the contours superimposed on the figure) in the H_α filter in 1996. The vectors show the amount of proper motion in a time interval of two (blue) and seven (red) years, respectively.

From the HST data sets reported in this paper, we can argue that the average speed of the knots at the base of the jet (the F-complex) over the last nine years is significantly lower (about a factor of 4; see Table 3) than the "instantaneous" speed over two years observed nine years before, suggesting a deceleration of this structure. The same is not valid in the case of the D knot, whose average speed increases about 26% with respect to the "instantaneous" speed derived about nine years before (see Table 3). Here there are indications of a slight acceleration of the D knot from 1998 to 2005, but it remains to be confirmed through later-epoch observations. The faintest knots within the jet, the E and the D_2 knots, disappeared in the 2005 observations (see discussion in Sect. 3.1), making it impossible to infer details concerning their dynamics.

The variation in the length of the jet as a whole is shown in Fig. 12, and the corresponding values are presented in Table 4 for each epochs in both filters. The length of the total jet is defined as the distance between the extremes of contours on "F-complex" (or knot F_2 if it is well-defined) and knot D. The average change in length found during this period (from 3 Feb. 1996 to 21-22 Feb. 2005 = 3306-3307 days) derived from the values in Table 4 is 0.082"/yr in H_α and 0.048"/yr in [SII], corresponding to a space velocity of about 58 km/s and 34 km/s, respectively.

3.4. Flux

To investigate the energetics describing the evolution of the knots within the HH 154 jet, we measured the fluxes inside the contours which define each structure in the jet (we used the same contours used in deriving the proper motion of the knots, as in Sect. 3.3). Our results are summarized in Table 5, where we present the total flux collected in the apertures around each single knot when it is well-defined (as in the case of knot D in both filters and for all the three epochs) or in the aperture containing multiple structures, as in the case of F-complex (in [SII] image in 1998 and H_α image in 2005, Fig. 5). The accuracy is computed adding in quadrature the measurement error and the precision in the flux calibration (5%, following Holtzman et al. 1995). Note that the apertures on each knot have different sizes for different epochs or filters. In fact, one of the main characteristic of the sub-structures within the jet is their rapid morphological evolution in few years.

The flux measured from the D knot decreases by 7% in [SII] from 1996 to 1998 and up to the 46% in H_α from 1996 to 2005. The same is true for the F and E knots, whose fluxes decrease by up to 6% and 51% in [SII], respectively. On the other hand, the fluxes of the F_2 and D_2 knots increase. An explanation of this result can be related to our choice of the contours defining the knots, which leads to larger apertures on these two knots, F_2 and D_2, in the epochs corresponding to higher fluxes. As said above, we are comparing fluxes within different areas in different epochs, because we are interested in following the evolution of the substructures in the jet, even their morphological variations. We therefore do not fix the areas of the knots through the epochs but let them change as the jet evolves. Computing the surface brightness of F_2 knot, as an example, we find that it decreases, thus leading to a 1998-to-1996 area ratio increasing faster than the corresponding fluxes ratio, and we can conclude that the increased flux observed stems from the increasing area, since the surface brightness itself decreases.

The total flux of the jet as a whole, defined as the sum of the fluxes of each knot and shown in Table 5, varies by decreasing from its maximum value of about 1.6×10^{-14} erg cm^{-2} s^{-1} in 1996 to its minimum of about 8.8×10^{-15} erg cm^{-2} s^{-1} in 2005 in the H_α filter, and from its maximum value of about 1.7×10^{-14} erg cm^{-2} s^{-1} in 1996 and 1998 to its minimum of about 1.3×10^{-14} erg cm^{-2} s^{-1} in 2005 in the [SII] filter. The contribution of the single knots to the total flux of the jet

[2] A procedure to this effect is available in SAOImage

Table 3. Proper motion computed for each knot within the jet.

Δt	Feature	displacement H_α	displacement [SII]	v@150 pc H_α	v@150 pc [SII]	v error	Comment
yr		arcsec	arcsec	km/s	km/s	km/s	
1998 - 1996	D	0.24	0.28	84	99	36	center[a]
1998 - 1996	D_2	0.35	0.46	125	165	36	center
1998 - 1996	E	0.38	0.46	134	164	36	center
1998 - 1996	F	0.39	0.28	138	100	36	max[b]
1998 - 1996	F_2	0.75	0.93	265	331	36	max
2005 - 1996	D	1.34	1.54	106	122	8	center
2005 - 1996	D_2	-	-	-	-	-	disappeared in 2005
2005 - 1996	E	-	-	-	-	-	disappeared in 2005
2005 - 1996	F	0.24	0.74	19	58	8	max
2005 - 1996	F_2	0.76	1.19	60	94	8	max

[a] Proper motion computed using the position of the center of the contour.
[b] Proper motion computed using the position of the maximum within the contour.

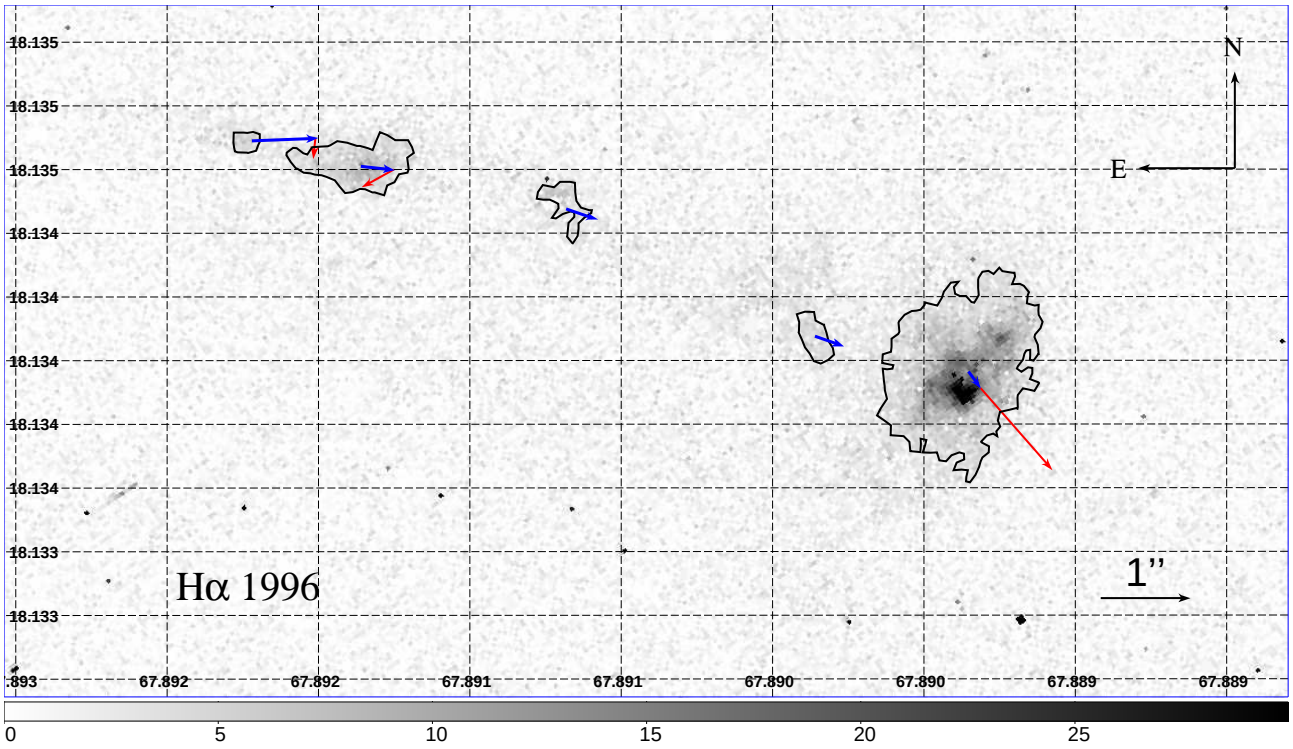

Figure 11. H_α image of HH 154 in 1996. The contours used to derive the proper motion of the knots within the jet are superimposed on the figure. The arrows show the distance traveled in two (blue) and in seven (red) years by each object, respectively, according to Table 3.

Table 4. The length of the jet at different epochs and in both H_α and [SII] filters computed as the distance between the extremes of contours on knots F_2 (or "F-complex" when there is a single contour for both F_2 and F knots) and knot D.

Filter	Year	Δt^*	Length	Rate of change	Rate of change@150 pc		v error
		days	arcsec	arcsec/yr	AU/yr	km/s	km/s
H_α	1996	0	9.53	-	-	-	-
H_α	1998	771	9.74	0.0997	15	71	36
H_α	2005	2535	10.27	0.0765	11	54	10
$[SII]$	1996	0	9.76	-	-	-	-
$[SII]$	1998	771	10.02	0.1234	19	88	36
$[SII]$	2005	2536	10.19	0.0245	4	17	10

[*] Number of days between successive epochs.

as a whole ranges from 2% for the faintest knots, D_2 and E, to 88% for the brightest knot, the terminal working surface, i. e.

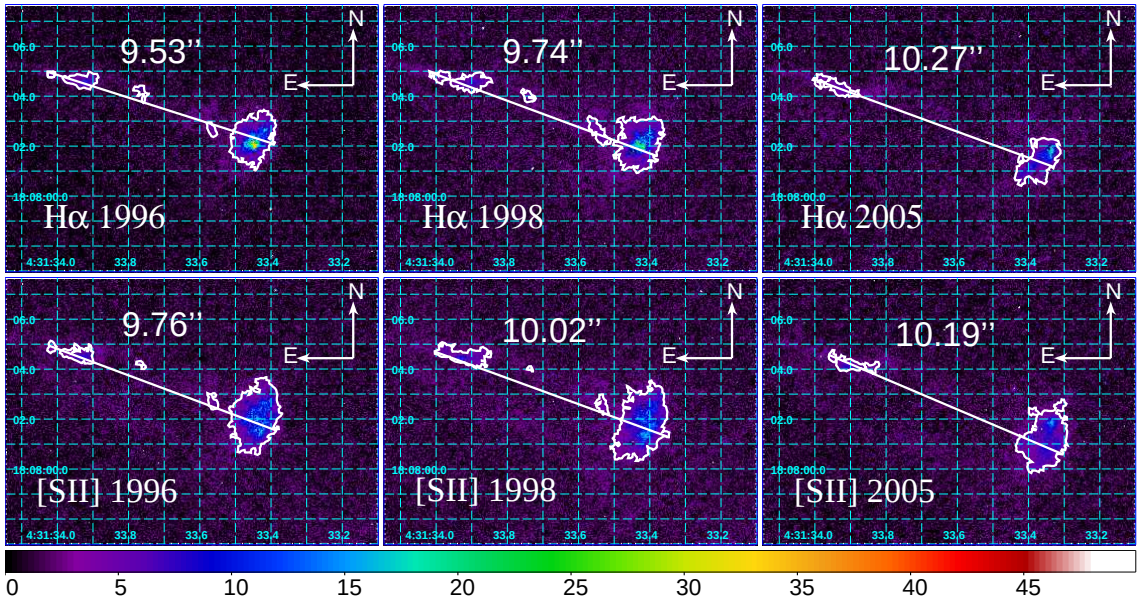

Figure 12. Total length of the HH 154 jet in 1996 (left panels), 1998 (middle panels), and 2005 (right panels) in H_α (upper panels) and [SII] (lower panels).

Table 5. Fluxes (erg cm^{-2} s^{-1}) and brightness of each knot within the jet and of the jet as a whole in H_α and [SII] filters for 1996, 1998, and 2005 HST observations.

Feature	flux[a] H_α	flux[a] $[SII]$	Source	Accuracy[a,b] (%)	brightness (10^{-15}) H_α	brightness (10^{-15}) $[SII]$
D	1.3×10^{-14}	1.5×10^{-14}	HST 1996	5.3 - 5.9	4.8	3.7
D_2	3.5×10^{-16}	3.7×10^{-16}	HST 1996	9.6 - 10.0	2.3	1.9
E	4.1×10^{-16}	8.9×10^{-17}	HST 1996	8.8 - 19.6	2.6	1.8
F	1.8×10^{-15}	1.6×10^{-15}	HST 1996	6.1 - 6.7	3.1	2.7
F_2	1.8×10^{-16}	2.1×10^{-16}	HST 1996	11.2 - 12.1	3.0	1.9
$F + F_2$	(2.0×10^{-15})	(1.8×10^{-15})	HST 1996	(5.7) - (6.1)		
Σ_{Alljet}	(1.6×10^{-14})	(1.7×10^{-14})	HST 1996	(4.5) - (5.2)		
D	1.1×10^{-14}	1.4×10^{-14}	HST 1998	6.3 - 6.2	3.6	3.1
D_2	8.4×10^{-16}	3.4×10^{-16}	HST 1998	9.0 - 11.1	1.9	1.5
E	2.9×10^{-16}	4.4×10^{-17}	HST 1998	11.2 - 19.3	1.8	1.5
F	1.8×10^{-15}	-	HST 1998	7.2	2.7	-
F_2	4.5×10^{-16}	-	HST 1998	11.1	1.9	-
$F + F_2$	(2.2×10^{-15})	2.3×10^{-15}	HST 1998	(6.2) - 7.3		2.1
Σ_{Alljet}	(1.4×10^{-14})	(1.7×10^{-14})	HST 1998	(4.9) - (5.3)		
D	7.0×10^{-15}	1.1×10^{-14}	HST 2005	6.8 - 6.3	3.5	3.2
D_2	-	-	HST 2005	-	-	-
E	-	-	HST 2005	-	-	-
F	-	1.5×10^{-15}	HST 2005	7.3	-	2.6
F_2	-	2.1×10^{-16}	HST 2005	11.8	-	2.1
$F + F_2$	1.8×10^{-15}	(1.7×10^{-15})	HST 2005	6.9 - (6.5)	2.7	
Σ_{Alljet}	(8.8×10^{-15})	(1.3×10^{-14})	HST 2005	(5.6) - (5.5)		

[a] The values in brackets are not measured within a single aperture containing the knots, but they are the sum of the values measured in single knots and the corresponding accuracy is computed using the addition in quadrature rule.
[b] The two values correspond to H_α and [SII] filters, respectively.

knot D. The flux of F-complex at the base of the jet contributes $(11-20)\%$ to the total flux.

4. Discussion

We first focus on the terminal working surface, identified with the D knot at the head of the jet. The H_α emission is interpreted as the emission originating in the Mach disk and the [SII] emission as due to the post-shock region just behind the

shock. Following the Hartigan (1989) model, a Mach disk significantly brighter than the bow shock, as evident in Fig. 9, is indicative of a jet traveling through a denser ambient medium, in good agreement with the Bonito et al. (2004, 2007) numerical results. In fact, one of the main result of their model is that only a narrow range of parameters of the jet/ambient system can reproduce the observations of protostellar jets. In particular only the scenario of a "light jet", i. e. the case of a jet traveling through a denser medium, can reproduce the observations of the HH 154 jet, and in particular the proper motion of the X-ray source, its emission, and spectral behavior. The separation observed between the centers of the contours defining the knot D in H_α and [SII] is about $0\farcs33$ (Fig. 9), consistent with the dimension of the width of the base of the jet. As in Hartigan (1989), the shock is radiative, the separation being close to the jet radius.

Unlike the other sub-structures within the HH 154 jet, the terminal working surface, identified as the D knot at the head of the jet, shows indications of acceleration (the velocity increases up to 26%) during the last seven years, i. e. from the 1998 observation to the last one in 2005. The fast D_2 knot (see its velocity in Table 3) disappeared in the 2005 HST observations (see Fig. 2). From this, we can argue that a collision between the two knots, D and D_2, may have occurred during the seven years between 1998, when the D_2 knot was still visible in both H_α and [SII] images of HH 154 (see Fig. 2), and in 2005. In fact we find that the D_2 could reach the D knot in about seven years and collide with it, since the minimum distance between the two knots in 1998 is about $0.6''$ and the relative speed is about $0.09''$/yr. Using the velocities shown in Table 3 and the density derived in FL05, assuming quasi-spherical knots for simplicity, we find, from the equation for momentum conservation in a totally inelastic collision, that the D_2 knot should be about 50 times denser than the D knot to explain a totally inelastic collision between the two knots, leading to the higher speed observed in the D knot in 2005. This collision between the two knots, D_2 and D, could also explain the detectable motion of the brightest spot observed within the D knot (Fig. 7).

The speed of the F and F_2 knots decreases from 1996 to 2005. Together with this time dependence of the velocity of the knots in the jet, there is also a dependence on the distance from the protostar along the jet axis ("space dependence"). In fact there is a clear decrease in the velocity derived in 1998 with increasing distance from the protostellar source IRS5, at the base of the jet, i. e. the maximum value of the knots speed is measured at the base of the jet, where the F_2 knot is, and then the speed decreases along the jet axis, reaching its minimum value at the head of the jet, corresponding to the terminal working surface, the D knot (Table 3). In particular, the velocity of the F_2 knot is almost three times higher than the D knot's speed. Both time and space dependence of the speed of the sub-structures within the jet can be used as a strong diagnostic power in detailed numerical simulations. In fact, as explained in Bonito et al. (2004, 2007), the shock formed at the interaction front between a supersonic protostellar jet and the surrounding medium travels at a velocity up to three times lower than the initial jet velocity in the case of a light jet, in particular the case of a jet ten times less dense than the ambient through which it propagates.

The direct measurements of the fluxes of each sub-structure within the HH 154 jet, in the three different epochs (1996, 1998, and 2005) and in both H_α and [SII] filters, allow us to derive important information concerning the dynamics of the knots in the jet. In particular, we can compare the variation in the fluxes in about two or nine years with the rate expected on the characteristic time scale of cooling by radiative losses, $\tau_{\rm cool} = 3nkTV/L$, where n is the density of the knot, k the Boltzmann constant, T the temperature of the knot, V its volume, and L the luminosity inferred from the measure of the flux as $L = 4\pi D^2 F$ (Table 5). Fridlund & Liseau (1998) found that the ionization fraction is probably close to 1, and FL05 found the following temperatures and densities from spectroscopic data for the D and F knots in [SII]: $T_e(D) = (8700 \pm 1000)$ K, $T_e(F) = (14250 \pm 1750)$ K, $n_e(D) = (1600 \pm 200)$ cm^{-3}, and $n_e(F) = (1800 \pm 200)$ cm^{-3}. These temperatures and densities are fairly well determined from the [SII]$6717/6731$Å ratio. They were, however, obtained from the ground, under seeing conditions of about 1 arcsec to 1.5 arcsec, so should be considered as averages over areas on the sky several times larger than the features discussed here. Given these uncertainties, we then derive a characteristic time scale for the radiative cooling, $\tau_{\rm cool} \approx 290$ yr for both knots.

We expect the fluxes of the knots to be reduced by a factor of 0.969 in nine years (from 1996 to 2005) and by a factor of 0.993 in two years (from 1996 to 1998). However, the ratio between the fluxes in the two epochs (i. e. F_{2005}/F_{1996} or F_{1998}/F_{1996}) are much lower than expected (in fact from Table 5 we derive: $F_{2005}/F_{1996} = 0.73$ and $F_{1998}/F_{1996} = 0.93$, for the D knot, and $F_{2005}/F_{1996} = 0.94$ for the F knot, while in 2005 the F knot cannot be identified within a single contour). Comparing the above results, we can conclude that the D and F knots cool down faster than expected (with the hypothesis that they are isothermal structures). These results suggest that the jet propagates turbulently into the surrounding medium and, as a consequence, a merging between the knot and the ambient medium is occurring. This process could reduce the emission from the knot faster than in the case of an isolated (i. e. not interacting with the surrounding) structure, so we are observing evidence of the strong interaction between the jet and the ambient through which it travels supersonically.

The ratio [SII]/H_α (Raga et al. 1996), indicates the level of excitation of all the substructures in the jet. In Table 6 we show the value of the excitation index for each knot in the three different epochs. Among all the substructures in the jet, only knot D, the working surface, shows an excitation index greater than 1.5 (in 2005), indicative of low-excitation emission; however, the [SII]/H_α ratio of the D knot varies in about nine years, ranging from 1.15, 1996, to 1.57, 2005. This behavior corresponds to an initial high-excitation emission from this structure, which is weakening with time. The opposite is true for the F-complex at the base of the jet, from which it is likely that the X-ray source observed with Chandra (Favata et al. 2006) originates. In fact, in the case of the F-complex, the excitation index varies from 1.17, in 1996, to 0.94, in 2005, indicative of high excitation increasing with time.

Table 6. The excitation index, defined as the ratio of [SII] to H_α flux (Raga et al. 1996), for the knots within the HH 154 jet for the three epochs, 1996, 1998, and 2005.

Feature	Year	[SII]/H_α^*	Accuracy (%)
D	1996	1.15	7.9
	1998	1.27	8.8
	2005	1.57	9.2
D_2	1996	1.06	13.9
	1998	0.40	14.3
	2005	-	-
E	1996	0.22	21.5
	1998	0.15	22.3
	2005	-	-
F	1996	0.89	9.1
	1998	-	-
	2005	-	-
F_2	1996	1.17	16.5
	1998	-	-
	2005	-	-
$F+F_2$	1996	(0.90)	
	1998	(1.00)	
	2005	(0.94)	

* The values in brackets are the sum of the values measured in single knots.

As shown in Sect. 3.2, at the base of the jet there is the indication of a new shock structure originating in the knot nearest to the protostar IRS5, the F-complex. In fact the stratification of the H_α and [SII] emission suggests the presence of a shock front, marked by the Balmer filament, and of the cooling zone, where the [SII] emission dominates as in the more evident terminal working surface (Fig. 9). The hypothesis of a new shock at the base of the jet can only be invoked for the 2005 $H_\alpha-$ [SII] difference image. In both 1996 and 1998 $H_\alpha-$ [SII] difference images, there is no clear evidence of a shock front, i. e. H_α and [SII] stratification, at the base of the jet. This result could be related to the activity of the protostar in which the jet originates, having a time scale on the order of few years, and can also be related to the evidence, described above, that the excitation increases with time near the base of the jet, where the F-complex is located and, more important, where the X-ray source was discovered (Bally et al. 2003). The location of the X-ray source from the HH 154 jet is actually very close to the position of the F-complex at the base of the jet itself, i. e. to the knot with highest proper motion (knot F_2, see Table 3). This is evident in Fig. 13, showing the X-ray source as detected with Chandra in 2005 with the optical knots' contours superimposed (left panel), and the H_α emission observed with HST in 2005 with the X-ray contours superimposed (right panel).

Acknowledgements. We would like to thank the referee, Prof. John Bally, for his comments and suggestions. R. B. would like to thank Dr. Marco Miceli for helpful discussions. This work makes use of results produced by the PI2S2 Project managed by the Consorzio COMETA, a project cofunded by the Italian Ministry of University and Research (MIUR) within the Piano Operativo Nazionale Ž01cRicerca Scientifica, Sviluppo Tecnologico, Alta Formazione Ž01d (PON 2000-2006). More information is available at http://www.pi2s2.it and http://www.consorzio-cometa.it.

References

Anderson, J. & King, I. R. 2003, PASP, 115, 113
Bally, J., Feigelson, E., & Reipurth, B. 2003, ApJ, 584, 843
Bieging, J. H. & Cohen, M. 1985, ApJ, 289, L5
Bonito, R., Orlando, S., Peres, G., Favata, F., & Rosner, R. 2004, A&A, 424, L1
Bonito, R., Orlando, S., Peres, G., Favata, F., & Rosner, R. 2007, A&A, 462, 645
Cudworth, K. M. & Herbig, G. 1979, AJ, 84, 548
Favata, F., Bonito, R., Micela, G., et al. 2006, A&A, 450, L17
Favata, F., Fridlund, C. V. M., Micela, G., Sciortino, S., & Kaas, A. A. 2002, A&A, 386, 204
Fridlund, C. V. M., Bergman, P., White, G. J., Pilbratt, G. L., & Tauber, J. A. 2002, A&A, 382, 573
Fridlund, C. V. M. & Liseau, R. 1998, ApJ, 499, L75
Fridlund, C. V. M., Liseau, R., Djupvik, A. A., et al. 2005, A&A, 436, 983
Hartigan, P. 1989, ApJ, 339, 987
Heathcote, S., Morse, J. A., Hartigan, P., et al. 1996, AJ, 112, 1141
Holtzman, J. A., Burrows, C. J., Casertano, S., et al. 1995, PASP, 107, 1065
Kenyon, S. J., Dobrzycka, D., & Hartmann, L. 1994, AJ, 108, 1872
Liseau, R., Fridlund, C. V. M., & Larsson, B. 2005, ApJ, 619, 959
Looney, L. W., Mundy, L. G., & Welch, W. J. 1997, ApJ, 484, L157+
Neckel, T. & Staude, H. J. 1987, ApJ, 322, L27
Raga, A. C., Böhm, K.-H., & Cantó, J. 1996, Revista Mexicana de Astronomia y Astrofisica, 32, 161
Rodriguez, L. F., Canto, J., Torrelles, J. M., & Ho, P. T. P. 1986, ApJ, 301, L25
Rodríguez, L. F., Curiel, S., Cantó, J., et al. 2003, ApJ, 583, 330
Rodríguez, L. F., D'Alessio, P., Wilner, D. J., et al. 1998, Nature, 395, 355
Snell, R. L., Loren, R. B., & Plambeck, R. L. 1980, ApJ, 239, L17
Vrba, F. J., Strom, S. E., & Strom, K. M. 1976, AJ, 81, 958

List of Objects

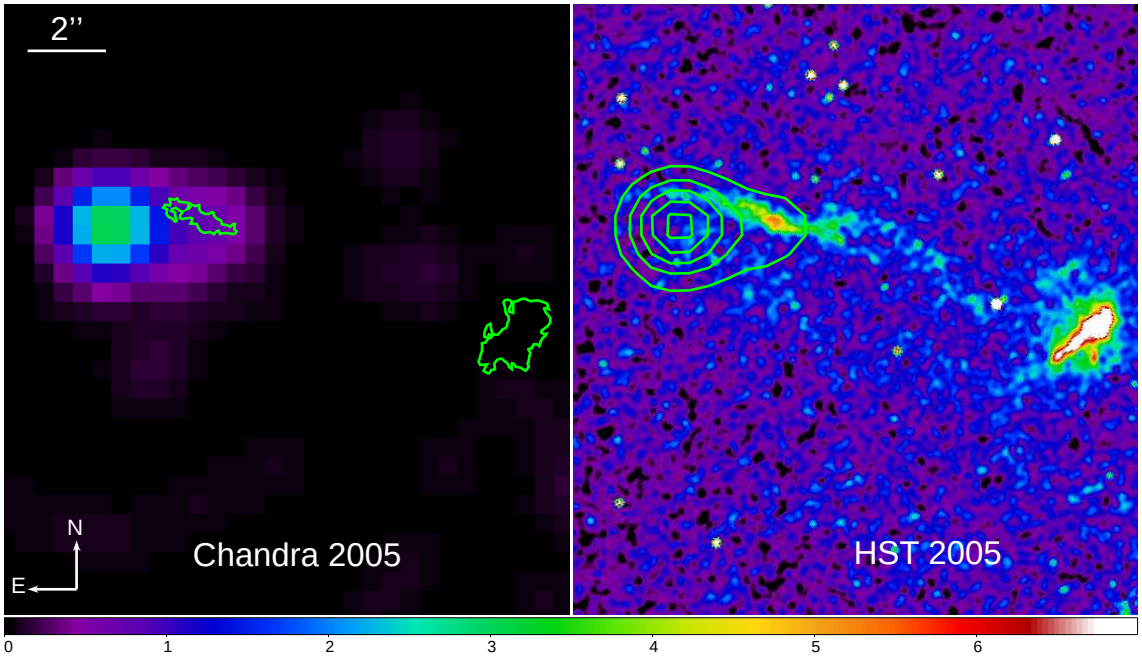

Figure 13. X-ray (left panel) and H_α (right panel) emission as detected with Chandra and Hubble, respectively. The contours of the optical knots and of the X-ray emission are superimposed on the X-ray and optical images, respectively.

‘IRS5’ on page 1
‘HH 154’ on page 2
‘HH 154’ on page 2
‘IRS5’ on page 2
‘IRS5’ on page 2
‘HH 154’ on page 2
‘IRS5’ on page 2
‘HH 154’ on page 2
‘L1551’ on page 2
‘IRS5’ on page 2
‘HH 154’ on page 2
‘HH 154’ on page 3
‘HH 154’ on page 4
‘IRS5’ on page 4
‘HH 154’ on page 4
‘IRS5’ on page 4
‘HH 154’ on page 4
‘IRS5’ on page 4
‘HH 154’ on page 4
‘HH 154’ on page 4
‘IRS5’ on page 4
‘HH 154’ on page 4
‘HH 154’ on page 4
‘HH 154’ on page 4
‘HH 154’ on page 5
‘HH 154’ on page 5
‘HH 154’ on page 5
‘IRS5’ on page 5
‘HH 154’ on page 6
‘HH 154’ on page 7
‘HH 154’ on page 7
‘IRS5’ on page 7
‘HH 154’ on page 7
‘HH 154’ on page 7
‘HH 154’ on page 7
‘HH 154’ on page 8
‘HH 154’ on page 8
‘HH 154’ on page 9
‘HH 154’ on page 10
‘HH 154’ on page 11
‘HH 154’ on page 11
‘HH 154’ on page 11
‘IRS5’ on page 11
‘HH 154’ on page 11
‘HH 154’ on page 12
‘IRS5’ on page 12
‘HH 154’ on page 12